ACS APPLIED MATERIALS & INTERFACES

Research Article

www.acsami.org

Transparent and Dense Ladder-Like Alkylene-Bridged Polymethylsiloxane Coating with Enhanced Water Vapor Barrier Property

Ce Zhang,[†,⊥] Cong Zhang,[†,⊥] Xinmin Cui,[†,⊥] Jinghua Sun,[†,⊥] Ruimin Ding,[‡] Qinghua Zhang,*[,§] and Yao Xu*[,‡]

[†]Key Laboratory of Carbon Materials, Institute of Coal Chemistry, Chinese Academy of Sciences, Taiyuan, Shanxi 030001, China

[‡]Xi'an Institute of Optics and Precision Mechanics, Chinese Academy of Sciences, Xi'an, Shaanxi 710119, China

[§]Chengdu Fine Optical Engineering Research Center, Chengdu, Sichuan 610041, China

[⊥]University of Chinese Academy of Sciences, Beijing 100049, China

Supporting Information

ABSTRACT: Organic−inorganic hybrid composites have been well-studied as water vapor barrier materials for their long diffusion length of water vapor in coatings which can be realized by improving the aspect ratio of inorganic components and regularity of nanostructure in coatings. In this paper, dense organic−inorganic hybrid coating based on ladder-like alkylene-bridged polymethylsiloxane (ABPMS) was successfully fabricated through the hydrosilylation reaction between polymethylhydrosiloxane and diene (1,5-hexadiene or 1,7-octadiene) in toluene under Pt/C catalysis. Its ladder-like structure was verified by ^{29}Si magic angle spinning (MAS) NMR, ^{13}C MAS NMR, and in-plane and out-of-plane glance-incident X-ray diffraction (GIXRD) techniques. Its corresponding coating showed excellent water vapor barrier ability for a typical water-soluble crystal, potassium dihydrogen phosphate (KDP). When treated in 50% relative humidity (RH) condition at 25 °C for 8 months, the ABPMS coating with 100 nm thickness displayed a very low transmittance loss of 1.6% compared with the high transmittance loss of 10% for uncoated KDP. Moreover, the ABPMS coating showed good ultraviolet radiation resistance, thermal stability, low mechanical property, and excellent compatibility with hydrophobic antireflective (AR) coatings.

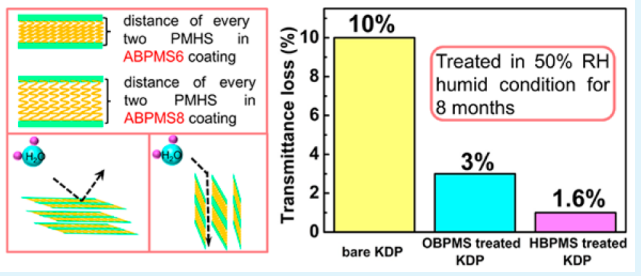

KEYWORDS: *water vapor barrier coating, dense coating, ladder-like polymer, alkylene-bridged polymethylsiloxane, hydrosilylation*

1. INTRODUCTION

Water vapor barrier coatings have attracted wide attention for their applications in food packages,[1,2] anticorrosion of metals,[3] stone restoration,[4] and protection of water-soluble optical crystals.[5−7] In order to prepare an efficient water vapor barrier coating, the effective method is to increase the diffusion pathway of water vapor in coatings, which can be realized by adding inorganic clay into polymer matrix or depositing inorganic nanoparticles on polymer coatings using the layer-by-layer deposition technique. For example, polylactide/montmorillonite has been widely investigated as water vapor barrier coatings[8] and can be obtained by melt-blending inorganic clay[9] or in situ crystallization[10] in polymer. Poly(lactic acid) treated by multilayers composed of a montmorillonite layer and a hydrophobic fluorinated polymer layer can also efficiently reduce water vapor transmission rate through coatings.[11] Those previous studies showed that a high aspect ratio of inorganic components[11] and ordered nanostructure[12] could obviously improve water vapor barrier ability of hybrid coatings by providing a long diffusion length of water vapor. However, it is difficult to avoid phase separation within coatings prepared by the above methods. In this work, our strategy of hybrid coatings with excellent water vapor barrier ability relied on the introduction of organic alkylene chains in a polymethylsiloxane matrix at the molecular level. To decrease phase separation and pinholes in hybrid coatings as much as possible, a ladder-like structure based on alkylene-bridged polymethylsiloxane is proposed here. According to this design, polymethylsiloxane containing a large amount of Si−O−Si bonding was used as inorganic backbone, and flexible alkylene chain was used as the organic component to link Si atoms in different polymethylsiloxane chains. As pinholes created between polymethylsiloxane chains can be filled by flexible alkylene through a chemical Si−C band, the ladder-like organic−inorganic hybrid tended to form a dense structure. Therefore, the alkylene-bridged ladder-like nanostructure is

Received: April 27, 2015
Accepted: September 22, 2015
Published: September 22, 2015

DOI: 10.1021/acsami.5b08084
ACS Appl. Mater. Interfaces 2015, 7, 22157−22165

expected to efficiently inhibit water vapor permeation through coating.

The selection of organic bridging monomer is vitally important. The coating containing light-absorbing organic groups, like benzene ring and ureylene groups, is easily photodegraded and loses water vapor barrier ability. For example, in Xu et al.'s work,[13] parylene used as water vapor barrier coatings could absorb the UV irradiation and subsequently be photodegraded. In Hu et al.'s work,[14] there were many ureylene groups in the coating which were easily decomposed under strong ultraviolet irradiation. As far as the ultraviolet radiation resistance of coatings is considered, chemical inert diene including 1,5-hexadiene and 1,7-octadiene will be used as bridging monomer in our work.

Up to now, the synthesis of hexylene-bridged polymethylsiloxane had been reported only by Kalfat and Gharbi[15] and Motoyama et al.[16] When they introduced 1,5-hexadiene into the polymethylsiloxane matrix through an uncontrolled reaction, the product tended to form a gel which could not be used to deposit the coating. In our work, the synthesis reaction of alkylene-bridged polymethylsiloxane (ABPMS) was investigated in detail, from which several suitable coating solutions were successfully fabricated by the Pt/C catalyzed hydrosilylation reaction between polymethylhydrosiloxane (PMHS) and 1,5-hexadiene (or 1,7-octadiene) in toluene, schematically shown in Figure 1. In this process, the catalyst Pt

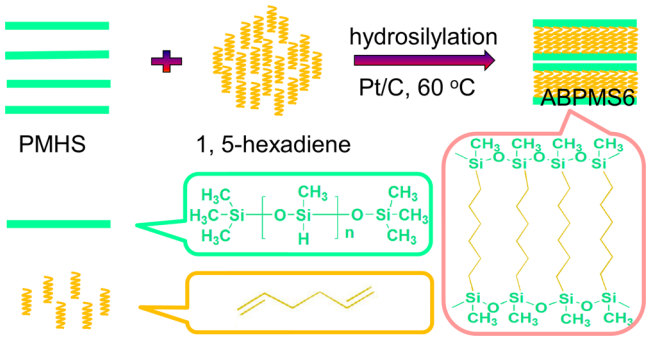

Figure 1. Synthesis scheme and ideal molecule structure of ABPMS, taking ABPMS6 for example.

was loaded on activated carbon for further easy removal from the coating solution by filtration after the completion of synthesis. Then, ABPMS with a ladder-like structure was confirmed by FT-IR ^{29}Si magic angle spinning (MAS) NMR and ^{13}C MAS NMR. Subsequently, ABPMS coating was deposited on potassium dihydrogen phosphate (KDP) crystal by a dip-coating method. The ordered structure in the ABPMS coating was studied by in-plane and out-of-plane glance-incident X-ray diffraction (GIXRD) techniques. The coating density was measured by X-ray reflectivity (XRR) methods. Then, the water vapor barrier ability was evaluated, and the corresponding water vapor barrier mechanism was proposed.

As a well-known nonlinear optical material that was extensively used for frequency conversion from 1053 to 351 nm wavelength in a high power laser system,[17,18] the KDP crystal was used to test the application of ABPMS. Therefore, the ultraviolet radiation resistance, thermal stability, and mechanical property of ABPMS coating were studied in detail. Besides, in order to improve the conversion efficiency of the KDP crystal, we also urgently needed a double-layer coating system possessing a water vapor barrier property as well as high optical transmittance at central wavelength of 1053 and 351 nm. Consequently, at the last part of this paper, ABPMS6 coating was overcoated by antireflective (AR) coatings with central wavelength of 1053 or 351 nm, and its improved transmittance was also investigated.

2. EXPERIMENTAL SECTION

2.1. Materials. All the reagents are commercially available and analytical grade. Chloroplatinic acid hexahydrate, ethanol, and zeolite were purchased from Sinopharm Chemical Reagent Co., Ltd. Toluene was provided by Tianjin Guangfu Company. Octadiene (97%) and hexadiene (98%) were bought from Alfa Company. Polymethylhydrosiloxane (PMHS, Mn = 1700−3200) was purchased from Aldrich Company. Tetraethylorthosilicate (TEOS) and 1,1,1,3,3,3-hexamethyldisilazane (HMDS) were purchased from Acros Company. All these were used without further purification except toluene. Toluene was dehydrated with zeolite before being used. The KDP crystal was purchased from Fujian Institute of Research on the Structure of Matter, Chinese Academy of Sciences.

2.2. Preparation of Pt/C Catalyst. Heterogeneous catalyst Pt/C was prepared by the incipient wetness technique using H_2PtCl_6/isopropanol solutions (concentration of H_2PtCl_6: 0.48 mmol/L) as metal precursor and activated carbon as carrier. Then, the Pt precursor was reduced by 37% formaldehyde solution. After the completion of reduction, Pt/C was filtrated by a Büchner funnel and then dried at 60 °C in vacuum for 12 h.

2.3. Synthesis of ABPMS. The ABPMS solution for deposition was synthesized using the following preparation. A stock solution (43 mL) of bridging monomer precursor was prepared by mixing diene (1,5-hexadiene or 1,7-octadiene), toluene, and Pt (Pt/C) = 1:63:0.0007 (molar ratio). The bridging monomer precursor solution was then added in a 250 mL three necked flask equipped with a condenser and vigorously stirred for 0.5 h at 60 °C to mix diene and catalyst thoroughly. A second solution of PMHS in 43 mL of toluene was added into the bridging monomer solution. The weight ratio of PMHS to toluene was 1:25. The final solution was kept stirring at 60 °C for several hours. During the course of the reaction, samples were taken and the hydrosilylation conversion was monitored by FT-IR. When the reaction completed, the Pt/C was removed by filtration. Here, it should be noted that the product with the bridging hexylene chain was marked as ABPMS6 and the other one with the bridging octylene chain was marked as ABPMS8. Thus, the obtained solution was used to deposit on the KDP crystal.

2.4. Synthesis of Silica Sol Modified by HMDS. Base-catalyzed silica sol was synthesized using the Stöber method.[19] The mixture solution was prepared by adding TEOS, EtOH, ammonia−water, and H_2O. The molar ratio of TEOS, EtOH, H_2O, and NH_3 was 1:38.2:2:0.1. Then, the solution was stirred for 2 h at 25 °C and then aged at 25 °C for 3 days. As modifier, HMDS was added into the above silica sol and aged at 25 °C for more than 7 days. The molar ratio of HMDS to silica was 1:2. Thus, obtained sol was diluted with the same volume of ethanol and then marked as HMDS-SiO_2 sol.

2.5. Deposition of Protective Coating. KDP crystals (23 × 23 × 8 mm^3) were cleaned with toluene before dip-coating. ABPMS6 or ABPMS8 was deposited on KDP crystals by the dip-coating technique at different withdraw rates to control the thickness of coatings. Thus, obtained coatings were marked as KDP//ABPMS6 or KDP//ABPMS8.

2.6. Deposition of Double-Layer Protective and Antireflective Coating. In double-layer coatings, the KDP//ABPMS6 protective coating was used as the bottom layer. HMDS-SiO_2 sol was deposited on these protective coatings by dip-coating at withdraw rates of 120 mm/min or 750 mm/min to set the central wavelength at 351 or 1053 nm. Thus, obtained coatings were marked as KDP//ABPMS6//AR351 or KDP//ABPMS6//AR1053, respectively.

2.7. Characterization of ABPMS. FT-IR was used to monitor the reaction between PMHS and dienes in toluene, which was recorded on a FT-IR spectrometer (IS50, Nicolet) using a KBr tablet. To further confirm the detailed molecular structure of ABPMS, ^{29}Si MAS NMR

DOI: 10.1021/acsami.5b08084
ACS Appl. Mater. Interfaces 2015, 7, 22157−22165

and ^{13}C MAS NMR spectra were conducted on a NMR spectrometer (AVANCE III 600 MHz, Bruker).

To measure the porosity of ABPMS, the powder was obtained from the ABPMS solution by removing toluene. Then, the specific surface area of ABPMS powder was measured on a physisorption analyzer (TriStar 3000, Micromeritics).

To confirm whether ABPMS powder adsorbed water vapor, the water vapor ad-desorption experiment was conducted on a dynamic gravimetric vapor sorption analyzer (DVS-Advantage, SMS). The ABPMS powder was dried in the DVS at 25 °C for 5 h. The relative humidity, RH, for samples was increased from 0% to 90% RH in 10% steps, with one more step of 5% increase from 90% RH to 95% RH. It was then decreased in a similar manner to accomplish a full sorption/desorption cycle. All the experimental partial pressure steps lasted for 3 h.

TG measurements were performed on a thermogravimetric analyzer (TGA, SDTA851, Mettler Toledo Star) in N_2 atmosphere. The temperature ranged from 25 to 1000 °C, with a temperature rate of 10 °C min^{-1} and gas flow of 500 mL min^{-1} on samples of about 12 mg. Decomposition temperatures T_{d5} and T_{d10} were determined for 5% and 10% weight losses, respectively.

2.8. Characterization of Coatings. The ordered structure of ABPMS coating on wafer was studied by in-plane and out-of-plane GIXRD patterns which were measured at BL14B1 beamline of SSRF in China with the X-ray wavelength of 0.124 nm. The density of ABPMS coating was calculated from the electronic density that was measured by XRR at 1W1A beamline of BSRF in China with the X-ray wavelength of 0.154 nm.[20−22] The electronic density of ABPMS coating was obtained by fitting the reflectivity data with a single-layer structural model.[23]

The plane and cross-sectional images of ABPMS coating was taken on a scanning electron microscope (SEM, JSM-7001F, JEOL). The transmittance values were measured on a UV−vis spectrometer (U-4100, Hitachi). The refractive index and the thickness of coatings were measured on a spectroscopic ellipsometry (SC620, Sanco).

The water vapor barrier ability of coatings was directly evaluated by comparing their optical transmittances before and after being treated in a 50% RH condition at 25 °C for 8 months. To more deeply understand the water vapor barrier mechanism, the water vapor transmission rate (WVTR) value was tested with a modified ASTM (1995) method E96. In this test, the ABPMS toluene solution was put on the surface of a sodium chloride saturated aqueous solution in a dish. After the solvent toluene vaporized, an ABPMS thin film was formed on the surface of the sodium chloride saturated solution. Then, this dish with ABPMS film was placed into a sealed desiccator in which there was a certain amount of anhydrous calcium chloride at 25 °C. Then, the weight change of anhydrous calcium chloride was recorded at different times (shown in Figure S1), and WVTR ($g{\cdot}d^{-1}{\cdot}m^{-2}$) was calculated from the slope of the straight line divided by the test ABPMS film area. The thickness of the coatings d (m) was 70 μm, measured from the cross-sectional SEM image of the ABPMS film (shown in Figure S2). When compared with other water vapor barrier coatings reported, the WVTR values in the references were normalized to one coating thickness of 70 μm using the following equation:

$$\text{normalized WVTR} = \text{nonnormalized WVTR} \times \frac{l}{70} \quad (1)$$

where l (μm) is the thickness of the film. All the reported WVTR values shown for comparisons were normalized.

The water contact angle of coatings was measured with a contact-angle meter (SL200B, CA). Ultraviolet radiation resistance was tested by putting bare KDP, KDP//ABPMS6, and KDP//ABPMS8 under a 300 W xenon lamp (PLS-SXE300, Perfectlight) with wavelength range of 250−380 nm for 3, 6, 9, and 12 h. The ultraviolet radiation resistance of coatings was evaluated by comparing the optical transmittances before and after being treated under ultraviolet radiation for different times. The mechanical properties including modulus and hardness of coatings were measured on a nanoindenter (G200, Agilent) with a diamond cube corner (three-sided pyramid) probe. The surface morphologies of coatings were analyzed on an atomic force microscope (AFM, XE-100, psia).

3. RESULTS AND DISCUSSION

3.1. Chemical Structure of ABPMS. As it is difficult to characterize the chemical structure of the coatings, ABPMS powder was characterized by FT-IR, ^{29}Si MAS NMR, and ^{13}C MAS NMR techniques. FT-IR was used to monitor the hydrosilylation reaction between Si−H and C═C groups. Because the only difference in chemical structure between ABPMS6 and ABPMS8 was the length of the alkylene chain, ABPMS6 was taken as an example. The IR spectra of ABPMS6 and PMHS are shown in Figure 2, in which both spectra show

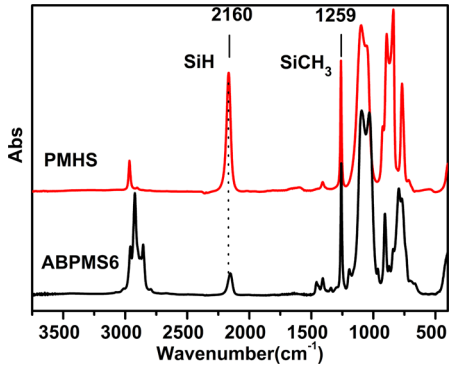

Figure 2. IR spectra of PMHS and ABPMS6.

absorption peaks at 2160 and 1259 cm^{-1} attributed to Si−H and Si-CH_3, respectively. For PMHS, the absorption intensity of Si−H and Si−CH_3 was approximately the same. After the completion of hydrosilylation, the absorption intensity of Si−H was much lower than that of Si−CH_3. As Si−CH_3 does not participate in the hydrosilylation reaction, it can conclude that most Si−H groups reacted with C═C groups. The conversion of hydrosilylation is about 83%, which is calculated using the equation: conversion = $100 \times (A_{(\text{PMHS, 2160})}/A_{(\text{PMHS, 1259})} - A_{(\text{ABPMS6, 2160})}/A_{(\text{ABPMS6, 1259})})/(A_{(\text{PMHS, 2160})}/A_{(\text{PMHS, 1259})})\%$. In this equation, $A_{(\text{PMHS, 2160})}$ and $A_{(\text{PMHS, 1259})}$ are integral absorption intensity of PMHS at 2160 and 1259 cm^{-1} and $A_{(\text{ABPMS6, 2160})}$ and $A_{(\text{ABPMS6, 1259})}$ are integral absorption intensity of ABPMS6 at 2160 and 1259 cm^{-1}. In addition, the existence of the C═C group (weak absorption peak at 1640 cm^{-1}) in the ABPMS6 spectra suggested that a small part of diene molecules had reacted with Si−H by only one C═C group.

The ^{29}Si MAS NMR spectra of the final product ABPMS6 is shown in Figure 3. A major resonance peak at −22.56 ppm was assigned to $-CH_2-{}^*Si(O-Si)_2CH_3$ (D unit).[24,25] The other two weaker peaks centered at 6.66 and −38.16 ppm indicated the existence of $Si-O-{}^*Si(CH_3)_3$ (M unit) and $H-{}^*Si(O-Si)_2CH_3$ (D^H unit), respectively. The M signal was assigned to the ending groups in PMHS. The major D signal occupied about 83% of the total peak area in the ^{29}Si NMR result, calculated using equation $D\% = 100 \times D/(D + D^H + D^{OH} + T)\%$, and the minor D^H signal occupied about 7% of the total peak area in the ^{29}Si MAS NMR result, which could be calculated by equation $D^H\% = 100 \times D^H/(D + D^H + D^{OH} + T)\%$. This result suggested that 83% of Si−H bonds reacted with C═C bonds except a little residue of the Si−H bonds. That is, the productiveness of ABPMS6 synthesis was 83%, which is the same as the estimated result of FT-IR. In addition,

DOI: 10.1021/acsami.5b08084
ACS Appl. Mater. Interfaces 2015, 7, 22157−22165

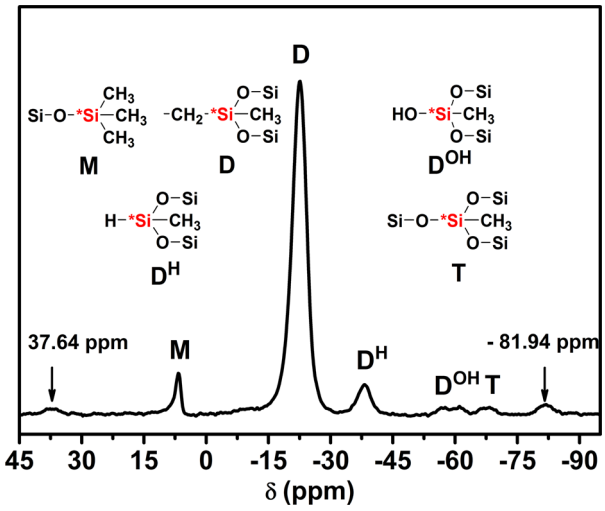

Figure 3. ^{29}Si MAS NMR spectra of ABPMS6, the spinning side bands were 37.64 and −81.94 ppm.

the existence of D^{OH} signal showed that some Si−H groups were hydrolyzed by water in air. Two Si−OH group units could condense into a Si−O−Si group of T unit shown in Figure 3.

To further confirm the structural details of bridging hexylene or octylene groups, the ^{13}C MAS NMR spectra of ABPMS6 and ABPMS8 were shown in Figure 4a,b. Because the bridging hexylene group had symmetry,[25] there are three distinct types of carbon atoms in a bridging group, marked as 1, 2, and 3 in Figure 4a. In ABPMS6, the signal at 18.26 ppm was attributed to the carbon C-1 closest to the Si atom. The C-2 and C-3 atoms corresponded to the signals at 23.49 and 33.55 ppm, respectively. Besides, the strongest peak in intensity appearing at 0.64 ppm was attributed to the C-4 atom in the methyl group in the PMHS chain. In addition, the two weakest peaks at 125.42 and 132.21 ppm were assigned to carbon atoms C-5 and C-6 of the unreacted CH═CH_2 group. However, the relative intensities of both C-5 and C-6 were far weaker than that of C-1 to C-4, showing the majority of Si−H groups had reacted with the two C═C groups in 1,5-hexadiene. For ABPMS8 shown in Figure 4b, there are four distinct types of carbon atoms in a bridging group, marked as 1, 2, 3, and 4. The signal at 18.55 ppm was attributed to the carbon C-1 closest to the Si atom. The C-2, C-3, and C-4 atoms corresponded to the signals at 23.84, 33.91, and 30.39 ppm, respectively. Besides, the strongest peak in intensity appearing at 0.54 ppm was attributed to the C-5 atom in the methyl group belonging to the PMHS chain. In addition, the two weakest peaks at 125.05 and 132.26 ppm were assigned to carbon atoms C-6 and C-7 of the unreacted CH═CH_2 group. Similar to ABPMS6, the relative intensities of both C-6 and C-7 were far weaker than that of C-1 to C-5, showing the majority of Si−H groups had reacted with the two C═C groups in 1,7-octadiene. On the basis of the above-mentioned FT-IR, ^{29}Si MAS NMR, and ^{13}C MAS NMR results, the chemical structure of ABPMS6 and ABPMS8 can be determined evidently.

3.2. Nanostructure of ABPMS Coating. The XRD patterns of ABPMS powder (shown in Figure S3) showed that both ABPMS6 and ABPMS8 had obvious ordered nanostructure. Accordingly, we schematically illustrate this ordered structure in Figure 5a. In Figure 5a, d_1 is the ladder width between two Si atoms bridged by the alkylene group and d_2 is the thickness of ladder. This ordered nanostructure may have two different orientations in the coating, parallel or perpendicular to the substrate (shown in Figure 5b), and the orientation information on the ABPMS coating can be obtained by the out-of-plane and in-plane GIXRD technique.

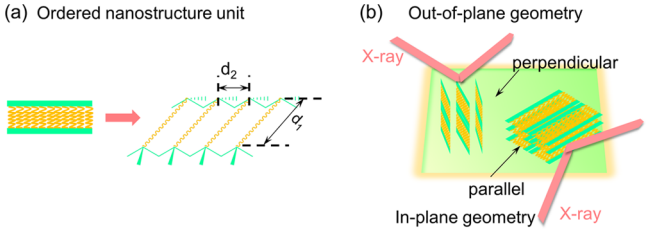

Figure 5. Schematic illustration of (a) ordered nanostructure unit and (b) GIXRD patterns of coating recorded in out-of-plane and in-plane geometries.

The out-of-plane and in-plane GIXRD patterns of ABPMS are shown in Figure 6a,b, respectively. In Figure 6a, ABPMS6 shows two broad bumps centered at about 11° and 20° corresponding to the d_1 of 8.0 Å and d_2 of 4.5 Å, respectively. d_1 is the ladder width formed by two Si atoms bridged by the hexylene group, and d_2 is the thickness of ladder illustrated by Figure 5a. However, the detected distance d_1 was shorter than the theoretical estimation 9.3 Å of the hexylene chain length, which could be attributed to the bending of the flexible bridging hexylene chain.[25,26] Also, as can be seen from Figure 5a, the d_1 value of ABPMS8 was 9.6 Å, larger than that of ABPMS6 because of the longer bridging octylene chain compared to the hexylene chain. However, ABPMS6 and ABPMS8 had the same

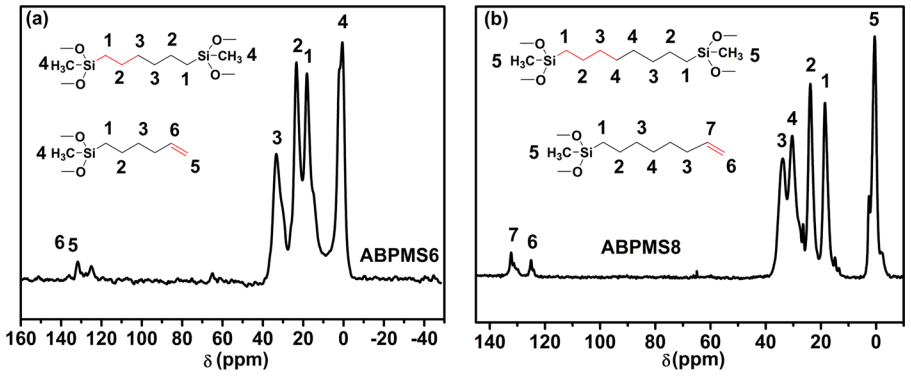

Figure 4. ^{13}C MAS NMR spectra of (a) ABPMS6 and (b) ABPMS8.

DOI: 10.1021/acsami.5b08084
ACS Appl. Mater. Interfaces 2015, 7, 22157−22165

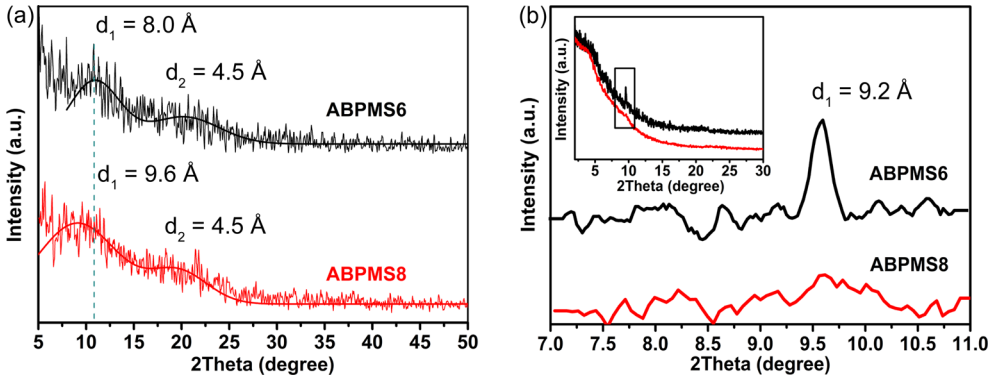

Figure 6. (a) Out-of-plane and (b) in-plane GIXRD patterns of ABPMS6 and ABPMS8 coatings.

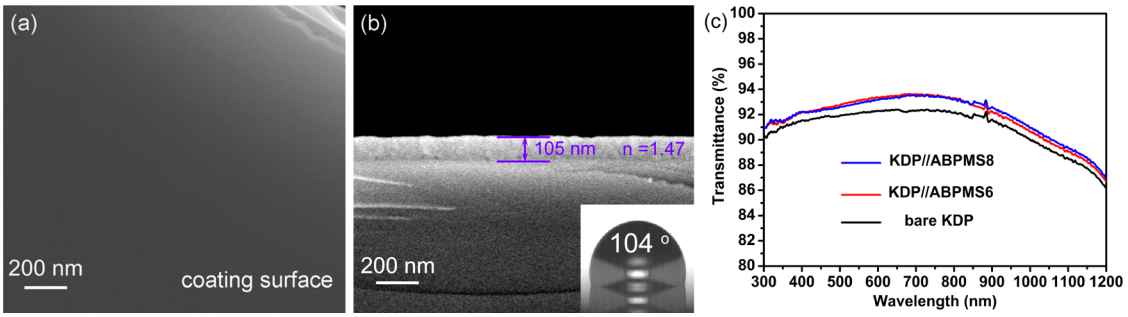

Figure 7. SEM images of (a) plane of ABPMS6 coating and (b) cross-section of ABPMS6 coating; (c) transmittance spectra of bare KDP (black), KDP//ABPMS6 (red), and KDP//ABPMS8 (blue).

d_2 value. In Figure 6b, the in-plane GIXRD pattern of the ABPMS6 coating displays a sharp peak centered at 9.6° corresponding d_1 = 9.2 Å which originated from the parallel ordered nanostructure. The d_1 could not be clearly seen in the in-plane GIXRD pattern of the ABPMS8 coating. This result indicated that the polymer orientation parallel to the substrate in the ABPMS6 coating was more perfect than that in the ABPMS8 coating. In other words, the ABPMS8 coating possessed less ordered nanostructures parallel to the substrate than the ABPMS6 coating, because longer bridging alkylene chain tended to collapse to form a disordered structure.[24] It is easier for the shorter bridging hexylene chain to keep the ordered nanostructure parallel to the substrate compared to the longer bridging octylene chain. Besides, the d_1 value in the in-plane GIXRD pattern of the ABPMS6 coating is larger than its counterpart in the out-of-plane geometry, suggesting that the bridging alkylene chain was arranged in a zip-like manner when perpendicular to the substrate and in a stretching manner when parallel to the substrate.

3.3. Water Vapor Barrier Property of ABPMS Coating.

According to our design, with ladder-like alkylene-bridged ordered nanostructures, ABPMS was thought to be dense. Measured by the XRR technique, the density of the ABPMS coating is around 1.16 g·cm^{-3}, much higher than the density of 0.65−0.80 g·cm^{-3} reported for the organic polysiloxane coating, a mixture of bis[trimethoxysilylpropyl]amine and vinyltriacetoxysilane coatings.[23] In order to further verify its dense structure, N_2 ad-desorption was conducted to measure the specific surface area of ABPMS. However, the specific surface area was too low to be detected, from which the microstructure of ABPMS was without open pores. Furthermore, the water vapor ad-desorption experiment was also done with ABPMS6 on a dynamic gravimetric vapor sorption analyzer. The result showed that ABPMS6 had no water vapor adsorption ability even in a 95% RH condition (shown in Figure S4).

Although the N_2 and water vapor ad-desorption results of ABPMS showed no open pores, it is necessary to confirm whether the coating possessed water vapor barrier ability. Then, an experiment of applying ABPMS to protect the water-soluble KDP crystal was designed to evaluate the water vapor barrier property of the ABPMS coating. In the experiment, the ABPMS coating was deposited on the KDP crystal by the dip-coating technique. Before the water vapor barrier test, the morphology of the ABPMS coating was well studied. As can be seen from Figure 7a, the surface of the ABPMS6 coating was smooth without obvious bumps, pinholes, and cracks, indicating that ABPMS6 had a good film-forming property. Moreover, in coating preparation, the thickness needed to be controlled to about 100 nm to avoid the interference of incident light in the ABPMS coating. As shown in Figure 7b, the thickness of the ABPMS6 coating is 105 nm, which was realized by controlling the withdraw rate of dip-coating at 35 mm/min. Then, the transmittance was measured on a UV−vis spectrometer with a wavelength range of 300−1200 nm and shown in Figure 7c. In Figure 7c, both ABPMS6 and ABPMS8 coatings show a little higher transmittance than the bare KDP crystal at the entire wavelength range, which could be explained by the lower refractive index of ABPMS6 and ABPMS8 coatings. According to the optical coating concept, the lower refractive index of the coating than that of the substrate can increase the transmittance of a transparent substrate.[27] Here, the refractive index of ABPMS6 and ABPMS8 coatings was 1.47 and 1.46, respectively, which was slightly lower than 1.46−1.51 of the KDP crystal.[28] Therefore, ABPMS6 and ABPMS8 coatings were helpful to the whole transmittance of the KDP crystal, and

DOI: 10.1021/acsami.5b08084
ACS Appl. Mater. Interfaces 2015, 7, 22157−22165

its good film-forming performance satisfied the optical demand of the water vapor barrier coating.

In the water vapor barrier test, three samples including bare KDP, KDP//ABPMS6, and KDP//ABPMS8 were treated in a 50% RH air condition at 25 °C for 8 months. The transmittance spectra of all samples before and after being treated in a 50% RH condition are shown in Figure 8. As can be seen from Figure 8a–c, the samples had different transmittance losses after being treated in a 50% RH condition for 8 months. In order to quantitatively compare the water vapor barrier property, transmittance loss ΔT was calculated and collected in Table 1. Because the working wavelengths of the KDP crystal as a frequency convertor were 351, 527, and 1053 nm, these two wavelengths were the focus. As is seen from Table 1, the transmittance of bare KDP displayed an obvious transmittance loss of around 10% at all central wavelengths after being treated in a 50% RH condition at 25 °C for 8 months. Meanwhile, KDP//ABPMS6 showed a transmittance loss of just around 1.6% after being treated in the same environment. With a longer alkylene bridging chain, KDP//ABPMS8 had a transmittance loss of a little higher than 3%. The water vapor barrier ability provided by ABPMS6 was obviously better than that by ABPMS8.

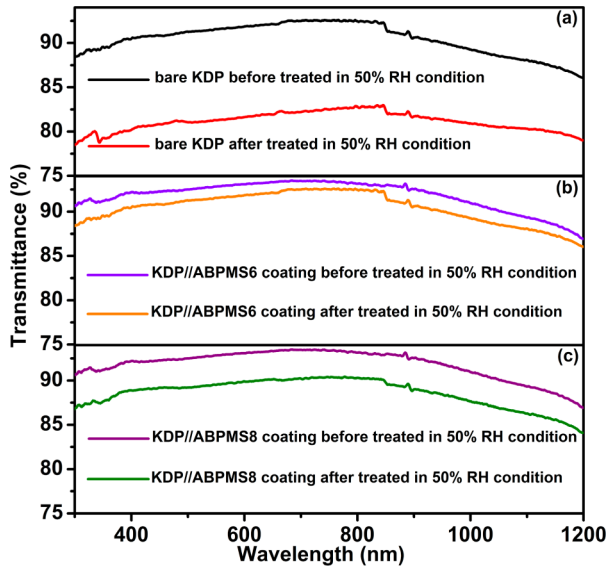

Figure 8. Transmittance spectra of (a) bare KDP, (b) KDP//ABPMS6, and (c) KDP//ABPMS8 before and after being treated in 50% RH at 25 °C for 8 months.

Table 1. Parameters of the Transmittance of Coatings at Different Wavelengths[a]

sample	351 nm ΔT (%)	527 nm ΔT (%)	1053 nm ΔT (%)
bare KDP	11.71	10.84	9.44
KDP//ABPMS6	1.67	1.63	1.54
KDP//ABPMS8	3.79	3.34	3.23

[a] ΔT is the transmittance loss after treating the KDP crystal with or without protective coating in a 50% RH condition at 25 °C for 8 months.

On the basis of the above analysis, both ABPMS6 coating and ABPMS8 coating performed good water vapor barrier protection to the KDP crystal although a small difference existed. Then, we tried to measure the WVTR value of the ABPMS coating using a modified ASTM (1995) method E96 that was usually used to characterize the water vapor diffusion length in a coating.[29] The thickness of the ABPMS self-standing film was about 70 μm measured from the cross-section SEM image (shown in Figure S2) in this experiment. For the ABPMS6 film, it exhibited WVTR of 71 $g \cdot d^{-1} \cdot m^{-2}$. At the same normalized thickness of 70 μm, our result was comparable to that of poly-L-lactide[12] (PLA, 14–138 $g \cdot d^{-1} \cdot m^{-2}$) and self-standing lamella siloxane-based hybrid coating (88 $g \cdot d^{-1} \cdot m^{-2}$) and much smaller than that of amorphous siloxane coating (571 $g \cdot d^{-1} \cdot m^{-2}$).[10] Consequently, the ABPMS6 film possessed very good water vapor barrier ability, but for the ABPMS8 film, the WVTR was as large as 469 $g \cdot d^{-1} \cdot m^{-2}$, which was 6 times larger than that of the ABPMS6 coating. Thus, the ABPMS6 coating displayed better water vapor barrier ability than that of the ABPMS8 coating.

Theoretically, the permeability of the water vapor molecule can be influenced by two aspects: the absorption and the diffusion. Generally, the absorption is controlled by the interaction between water molecules and polymer matrix, and the diffusion depends on the coating microstructure.[30] ABPMS6 and ABPMS8 coatings possessed the same water contact angle of 104°, indicating the same surface energy of ABPMS6 and ABPMS8 coatings. Considering nonabsorption of water vapor verified by the above-mentioned water vapor ad-desorption experiment, it can be concluded that ABPMS6 and ABPMS8 coatings had no water vapor absorption ability. The water vapor absorption can be excluded. Therefore, we attributed the different water vapor barrier property to the diffusion mechanism that is influenced by their different microstructures. On the basis of the GIXRD results mentioned above, there were two reasons to explain the differences. On one hand, the longer bridging alkylene chain could extend the ladder width of the ladder-like polymer (verified by the out-of-plane GIXRD result), which might form bigger voids in the coating shown in Figure 9a; i.e., the ABPMS6 coating should be

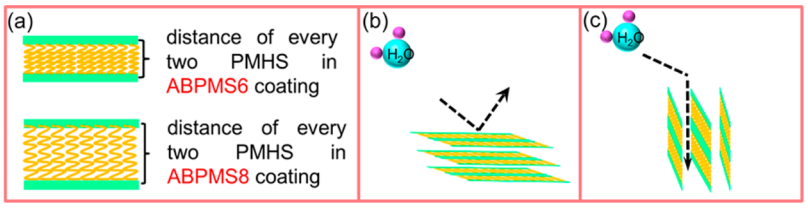

Figure 9. Schematic representation of (a) ordered nanostructure in the ABPMS6 coating and the ABPMS8 coating, respectively, (b) water vapor barrier mechanism of ordered nanostructure parallel to the substrate, and (c) water vapor barrier mechanism of ordered nanostructure perpendicular to the substrate. The motion pathway of a water molecule is illustrated with the black dotted line.

DOI: 10.1021/acsami.5b08084
ACS Appl. Mater. Interfaces 2015, 7, 22157–22165

denser than the ABPMS8 coating. On the other hand, the ordered nanostructures with different orientations in coating can also influence the diffusion pathway of the water vapor molecule through the coating, as illustrated schematically in Figure 9b,c, respectively. When ordered nanostructures are parallel to the substrate, they seem to repel water vapor off of the ABPMS surface (shown in Figure 9b), but when ordered nanostructures are perpendicular to the substrate, they seem to enable water vapor to diffuse through the lamellar voids formed by the adjacent two ordered nanostructures (shown in Figure 9c). Therefore, the ordered nanostructures parallel to the substrate can efficiently be a barrier to the water vapor compared to that perpendicular to the substrate. According to the in-plane GIXRD result, the ABPMS6 coating, with more ordered nanostructures parallel to the substrate, displayed a much better water vapor barrier performance than that of the ABPMS8 coating with less ordered nanostructures parallel to the substrate. In conclusion, a smaller ladder width and ordered nanostructure parallel to the substrate efficiently enhanced the water vapor barrier ability of the ABPMS coating.

3.4. Ultraviolet Radiation Resistance and Thermal Stability of Coatings. As water vapor barrier coatings for KDP, the ultraviolet radiation resistance and thermal stability of ABPMS6 and ABPMS8 coatings are important properties for their practical application. The transmittance change of bare KDP, KDP//ABPMS6, and KDP//ABPMS8 at 351 nm after being irradiated by ultraviolet lamps of 300 W for different times is shown in Figure S5. As can be seen from Figure S5, ABPMS6 and ABPMS8 coatings showed no transmittance loss after being irradiated for 12 h, indicating that ABPMS6 and ABPMS8 coatings are stable under strong ultraviolet irradiation. The thermogravimetric analysis result shows that both ABPMS6 and ABPMS8 displayed similar degradation profiles from 25 to 1000 °C under N_2 flow (shown in Figure S6). T_{d5} and T_{d10} of ABPMS6 were 444 and 470 °C, respectively, and for ABPMS8, T_{d5} and T_{d10} were 444 and 467 °C, respectively. These temperatures were much higher than that of polysilsesquioxane. For example, the T_{d5} of 394 °C and T_{d10} of 438 °C were reported for polysilsesquioxane containing phthalimido side-chain groups,[31] and the T_{d5} of 351 °C and T_{d10} of 368 °C were reported for polyhedral oligomeric silsesquioxane.[32] Therefore, the ABPMS coating had very good thermal stability which was attributed to the ladder-like alkylene-bridged structure.

3.5. Mechanical Property of ABPMS Coating. Young's modulus and hardness of coatings are two important mechanical properties, and they were measured and calculated with a nanoindentation technique. For the ABPMS6 coating, its Young's modulus and hardness were 0.2 and 0.01 GPa, respectively. While for the ABPMS8 coating, they were 0.3 and 0.02 GPa, a little higher than that of the ABPMS6 coating. However, they were much lower than 4.7 and 0.8 GPa reported for other polymer/clay composites.[20] It is well-known that linear polysiloxane is a good plasticizer and can decrease the modulus by its plasticizing effect in the polymer matrix.[33] Polysiloxane as a main ladder frame in the ladder-like ABPMS polymer intrinsically decreases the Young's modulus and hardness of ABPMS coatings. Despite the low Young's modulus and hardness of the ABPMS coating, it can effectively cushion the impact of external forces.

3.6. Enhanced Optical Transmittance of ABPMS6 and AR Coating. On the basis of the above results, the ABPMS6 coating displayed an excellent water vapor barrier property, good ultraviolet radiation resistance, good thermal stability, and low mechanical property. However, as a practical water vapor barrier coating for the KDP crystal, it should also have transmittance as high as possible at the conversion wavelengths, 351 and 1053 nm.[34] Then, the compatibility of ABPMS6 and a commonly used antireflective silica coating should be well studied. With the consideration of the compatibility with the hydrophobic ABPMS6 coating, silica nanoparticles modified by HMDS were used to deposit antireflective coating on the ABPMS6 coating (shown in Figure S7a). Because a single layer quarterwave sol−gel silica AR coating can only give maximum transmittance at a designed central wavelength, the AR coatings for KDP should be centered at 351 and 1053 nm wavelength which could be easily realized by adjusting the thickness of AR coatings. Figure 10 shows the transmittance curves of bare

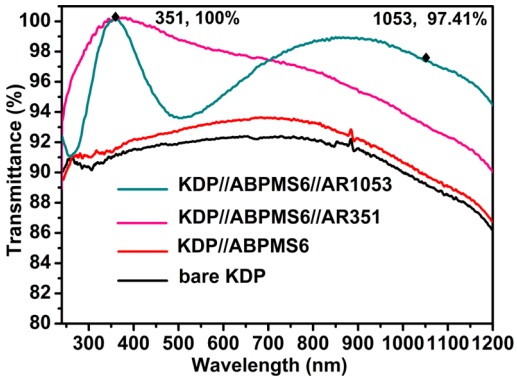

Figure 10. Transmittance spectra of bare KDP, KDP//ABPMS6, KDP//ABPMS6//AR351, and KDP//ABPMS6//AR1053.

KDP, KDP//ABPMS6, KDP//ABPMS6//AR351, and KDP//ABPMS6//AR1053. For KDP//ABPMS6//AR351, the transmittance at 351 nm is 100%. In KDP//ABPMS6//AR1053, the transmittance at 1053 nm is 97.4% much lower than the expected transmittance of 100%, which resulted from the special nonlinear optical property of the KDP crystal. However, the transmittance at 351 nm can reach 100% in KDP//ABPMS6//AR1053. Therefore, the double-layer KDP//ABPMS6//AR1053 is more suitable for protective and antireflective application for the KDP crystal. The boundary between the AR coating and the HBPMS coating was clear (shown in Figure S7b,c), suggesting that the bottom layer was dense and silica nanoparticles in the AR coating did not penetrate into the bottom layer. In addition, the HMDS−SiO_2 antireflective coating was hydrophobic with a water contact angle of 126° (shown in Figure S7b,c), which can easily repel water to improve the environmental stability of the KDP crystal.[6]

3.7. Morphologies of Coatings. Figure 11 shows the morphologies of bare KDP, the ABPMS6 coating, and the AR coating, which were tested with atomic-force microscopy. The morphologies of bare KDP and ABPMS6 coating were smooth and the roughness Rq was 0.5 and 1.2 nm, respectively. The roughness Rq of the ABPMS6 coating was a little higher than that of bare KDP. Thus, a smooth surface did not result in intense light scattering.[35] Unlike the ABPMS6 coating, there were many particle-like bumps on the surface of the AR coating (shown in Figure 11c). Therefore, the roughness Rq of AR coatings was 2.9 nm higher than that of the ABPMS6 coating.

DOI: 10.1021/acsami.5b08084
ACS Appl. Mater. Interfaces 2015, 7, 22157−22165

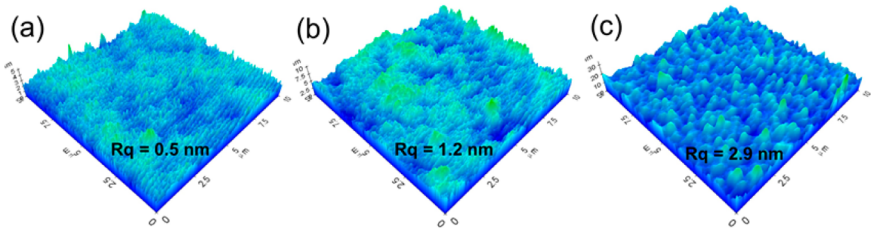

Figure 11. AFM images of (a) bare KDP, (b) ABPMS6 coating, and (c) ABPMS6//AR on the KDP crystal.

4. CONCLUSIONS

In summary, the ladder-like polymer ABPMS solution was successfully prepared by the hydrosilylation reaction. Its dense ladder-like alkylene-bridged structure could efficiently be a barrier for water vapor. Moreover, its corresponding coating exhibited excellent ultraviolet radiation resistance, thermal stability, low mechanical property, and good compatibility with hydrophobic AR coatings, which made it more potential as a water vapor barrier coating for a water-soluble crystal. Furthermore, the concept of introducing an organic bridging chain into an inorganic polysiloxane matrix provides a method to fabricate organic−inorganic material with a dense structure and an excellent water vapor or other gas barrier property.

■ ASSOCIATED CONTENT

Supporting Information

The Supporting Information is available free of charge on the ACS Publications website at DOI: 10.1021/acsami.5b08084.

Additional information about the WVTR measurement result, cross-sectional SEM image of ABPMS self-standing film, XRD patterns of ABPMS6 and ABPMS8, water ad-desorption isotherm cycle for ABPMS6, schematic representation of the structure of the double-layer system KDP//ABPMS6//AR, and SEM images of the cross-section of ABPMS6//AR351 and ABPMS6//AR1053. (PDF)

■ AUTHOR INFORMATION

Corresponding Authors

*E-mail: xuyao@sxicc.ac.cn.
*E-mail: zhangqh506@163.com.

Notes

The authors declare no competing financial interest.

■ ACKNOWLEDGMENTS

The work was supported by the Natural Science Foundation of China (No. U1530148). We also thank Prof. Yi Liu for his help in the out-of-plane and in-plane GIXRD measurements.

■ REFERENCES

(1) Martini, S.; Kim, D. A.; Ollivon, M.; Marangoni, A. G. The Water Vapor Permeability of Polycrystalline Fat Barrier Films. *J. Agric. Food Chem.* **2006**, *54*, 1880−1886.
(2) Han, J.; Salmieri, S.; Le Tien, C. L.; Lacroix, M. Improvement of Water Barrier Property of Paperboard by Coating Application with Biodegradable Polymers. *J. Agric. Food Chem.* **2010**, *58* (5), 3125−3131.
(3) Pan, G. R.; Watkins, E.; Majewski, J.; Schaefer, D. W. Effect of Thickness on the Water-Barrier Properties of Silane Films. *J. Phys. Chem. C* **2007**, *111*, 15325−15330.
(4) Mosquera, M. J.; de los Santos, D. M.; Rivas, T. Surfactant-Synthesized Ormosils with Application to Stone Restoration. *Langmuir* **2010**, *26* (9), 6737−6745.
(5) Hu, S. W.; Yang, D. J.; Xu, Y.; Wu, D.; Sun, Y. H. A Novel Moisture-Resistant Film for $NiSO_4{\cdot}6H_2O$ Filter Based on Isophorone Diisocyanate-Bridged Polysilsesquioxane. *Mater. Chem. Phys.* **2009**, *114*, 868−873.
(6) Zhang, X. X.; Ye, H. P.; Xiao, B.; Yan, L. H.; Lv, H. B.; Jiang, B. Sol-Gel Preparation of PDMS/Silica Hybrid Antireflective Coatings with Controlled Thickness and Durable Antireflective Performance. *J. Phys. Chem. C* **2010**, *114*, 19979−19983.
(7) Xiong, H. A.; Li, H. Y.; Tang, Y. X. Sol-Gel Derived Moisture-Resistant Antireflective Coatings for Potassium Dihydrogen Phosphate (KDP) Crystals. *Rare Met. Mater. Eng.* **2010**, *39*, 224−227.
(8) Thellen, C.; Orroth, C.; Froio, D.; Ziegler, D.; Lucciarini, J.; Farrell, R.; D'Souza, N.; Ratto, J. A. Influence of Montmorillonite Layered Silicate on Plasticized Poly(l-lactide) Blown Films. *Polymer* **2005**, *46* (25), 11716−11727.
(9) Kontou, E.; Niaounakis, M.; Georgiopoulos, P. C. Study of PLA Nanocomposites Reinforced with Clay and Silica Nanofillers and Their Mixtures. *J. Appl. Polym. Sci.* **2011**, *122* (3), 1519−1529.
(10) Tokudome, Y.; Hara, T.; Abe, R.; Takahashi, M. Transparent and Robust Siloxane-Based Hybrid Lamella Film as a Water Vapor Barrier Coating. *ACS Appl. Mater. Interfaces* **2014**, *6* (21), 19355−19359.
(11) Carosio, F.; Colonna, S.; Fina, A.; Rydzek, G.; Hemmerle, J.; Jierry, L.; Schaaf, P.; Boulmedais, F. Efficient Gas and Water Vapor Barrier Properties of Thin Poly(lactic acid) Packaging Films: Functionalization with Moisture Resistant Nafion and Clay Multilayers. *Chem. Mater.* **2014**, *26* (19), 5459−5466.
(12) Tsuji, H.; Tsuruno, T. Water Vapor Permeability of Poly(L-lactide)/Poly(D-lactide) Stereocomplexes. *Macromol. Mater. Eng.* **2010**, *295* (8), 709−715.
(13) Chao, X.; Jun, S.; Bin, Z.; Guangming, W.; Xiang, X. Study on Parylene/SiO_2 Composite Films for Protection of KDP Crystals. *J. Sol-Gel Sci. Technol.* **2008**, *45*, 319−324.
(14) Hu, S. W.; Xu, Y.; Jiang, D.; Wu, D.; Sun, Y. H.; Deng, F. Moisture-Resistant Protective Films for UV-Light Filter Based on Diisocyanate-Bridged Polysilsesquioxanes. *Thin Solid Films* **2009**, *518* (1), 348−354.
(15) Kalfat, R.; Gharbi, N. Synthesis and Thermal Behavior of Gels Obtained by Chemical Modification of Polymethylsiloxane by Vinyl and Diols. *J. Mater. Synth. Process.* **1994**, *2* (6), 379−387.
(16) Motoyama, Y.; Kamo, K.; Nagashima, H. Catalysis in Polysiloxane Gels: Platinum-Catalyzed Hydrosilylation of Polymethylhydrosiloxane Leading to Reusable Catalysts for Reduction of Nitroarenes. *Org. Lett.* **2009**, *11* (6), 1345−1348.
(17) Mei, Y.; Peng, R.-M.; Wei, F.; Zheng, W. C. Spin-Hamiltonian Parameters and Local Structures of the Tetragonal $(CrO_4)^{3-}$ Clusters in Cr^{5+}-doped KDP-type Crystals. *Opt. Mater.* **2014**, *36*, 1250−1254.
(18) Rajesh, P.; Silambarasan, A.; Ramasamy, P. Effect of Crystal Violet Dye on the Optical, Dielectric, Thermal and Mechanical Properties of < 001> Directed KDP Single Crystal. *Mater. Res. Bull.* **2014**, *49*, 640−644.
(19) Stober, W.; Fink, A.; Bohn, E. Controlled Growth of Monodisperse Silica Spheres in Micron Size Range. *J. Colloid Interface Sci.* **1968**, *26* (1), 62−69.

DOI: 10.1021/acsami.5b08084
ACS Appl. Mater. Interfaces 2015, 7, 22157−22165

(20) Lionti, K.; Cui, L.; Volksen, W.; Dauskardt, R.; Dubois, G.; Toury, B. Independent Control of Adhesive and Bulk Properties of Hybrid Silica Coatings on Polycarbonate. *ACS Appl. Mater. Interfaces* **2013**, *5*, 11276−11280.
(21) Cui, L.; Lionti, K.; Ranade, A.; Larson-Smith, K.; Dubois, G.; Dauskardt, R. Highly Transparent Multifunctional Bilayer Coatings on Polymers Using Low-Temperature Atmospheric Plasma Deposition. *ACS Nano* **2014**, *8*, 7186−7191.
(22) Cui, L.; Ranade, A. N.; Matos, M. A.; Pingree, L. S.; Frot, T. J.; Dubois, G.; Dauskardt, R. H. Atmospheric Plasma Deposited Dense Silica Coatings on Plastics. *ACS Appl. Mater. Interfaces* **2012**, *4*, 6587−6598.
(23) Wang, Y. M.; Watkins, E.; Ilavsky, J.; Metroke, T. L.; Wang, P.; Lee, B.; Schaefer, D. W. Water-Barrier Properties of Mixed Bis[trimethoxysilylpropyl]amine and Vinyltriacetoxysilane Films. *J. Phys. Chem. B* **2007**, *111*, 7041−7051.
(24) Loy, D. A.; Obrey-DeFriend, K. A.; Wilson, K. V., Jr.; Minke, M.; Baugher, B. M.; Baugher, C. R.; Schneider, D. A.; Jamison, G. M.; Shea, K. J. Influence of the Alkoxide Group, Solvent, Catalyst, and Concentration on the Gelation and Porosity of Hexylene-Bridged Polysilsesquioxanes. *J. Non-Cryst. Solids* **2013**, *362*, 82−94.
(25) Thami, T.; Nasr, G.; Bestal, H.; Van Der Lee, A.; Bresson, B. Functionalization of Surface-Grafted Polymethylhydrosiloxane Thin Films with Alkyl Side Chains. *J. Polym. Sci., Part A: Polym. Chem.* **2008**, *46* (11), 3546−3562.
(26) Guo, G. Q.; Zhang, Y.; Li, H.; Xie, P.; Zhang, R. B. Synthesis of a Novel 2,5-Dipropylhydroquinone-Bridged Ladder-Like Polymethylsiloxane Using a Hydroquinone H-Bonding Self-Assembling Template. *Macromol. Rapid Commun.* **2002**, *23*, 366−369.
(27) Schallenberg, U. B. Antireflection Design Concepts with Equivalent Layers. *Appl. Opt.* **2006**, *45*, 1507−1514.
(28) Thomas, I. M.; Campbell, J. H. A Novel Perfluorinated AR and Protective Coating for KDP and Other Optical-Materials. *Proc. SPIE* **1990**, *1441*, 294−303.
(29) Garcia, M.; Pinotti, A.; Martino, M.; Zaritzky, N. Characterization of Composite Hydrocolloid Films. *Carbohydr. Polym.* **2004**, *56*, 339−345.
(30) Ho, T. T.; Zimmermann, T.; Ohr, S.; Caseri, W. R. Composites of Cationic Nanofibrillated Cellulose and Layered Silicates: Water Vapor Barrier and Mechanical Properties. *ACS Appl. Mater. Interfaces* **2012**, *4*, 4832−4830.
(31) Miyauchi, S.; Sugioka, T.; Sumida, Y.; Kaneko, Y. Preparation of Soluble Polysilsesquioxane Containing Phthalimido Side-Chain Groups and Its Optical and Thermal Properties. *Polymer* **2015**, *66*, 122−126.
(32) Tokunaga, T.; Koge, S.; Mizumo, T.; Ohshita, J.; Kaneko, Y. Facile Preparation of A Soluble Polymer Containing Polyhedral Oligomeric Silsesquioxane Units in Its Main Chain. *Polym. Chem.* **2015**, *6*, 3039−3045.
(33) Ramezanzadeh, B.; Moradian, S.; Tahmasebi, N.; Khosravi, A. Studying the Role of Polysiloxane Additives and Nano-SiO_2 on the Mechanical Properties of a Typical Acrylic/Melamine Clearcoat. *Prog. Org. Coat.* **2011**, *72*, 621−631.
(34) Thomas, I. M. Optical and Environmentally Protective Coatings for Potassium Dihydrogen Phosphate (KDP) Harmonic Converter Crystals. *Proc. SPIE* **1991**, *1624*, 70−82.
(35) Tian, G.; Dong, L.; Wei, C.; Huang, J.; He, H.; Shao, J. Investigation on Microstructure and Optical Properties of Titanium Dioxide Coatings Annealed at Various Temperature. *Opt. Mater.* **2006**, *28* (8−9), 1058−1063.

DOI: 10.1021/acsami.5b08084
ACS Appl. Mater. Interfaces 2015, 7, 22157−22165